ACS Catalysis

Research Article

pubs.acs.org/acscatalysis

Evaluating Electrocatalysts for the Hydrogen Evolution Reaction Using Bipolar Electrode Arrays: Bi- and Trimetallic Combinations of Co, Fe, Ni, Mo, and W

Stephen E. Fosdick,[†,§] Sean P. Berglund,[‡,§] C. Buddie Mullins,*[,†,‡] and Richard M. Crooks*[,†]

[†]Department of Chemistry and the Center for Nano- and Molecular Science and Technology, The University of Texas at Austin, 105 East 24th Street, Stop A5300, Austin, Texas, 78712-0165, United States

[‡]McKetta Department of Chemical Engineering, The University of Texas at Austin, 200 East Dean Keeton Street, Stop C0400, Austin, Texas 78712-1589, United States

Supporting Information

ABSTRACT: Here, we report the development of a parallel electrocatalyst screening platform for the hydrogen evolution reaction (HER) using bipolar electrodes (BPEs). Electrocatalyst candidates are subjected to screening in a N_2-purged bipolar electrochemical cell where a pair of driving electrodes produce an electric field in the electrolyte solution. The HER occurring at the BPE cathodes is electrically coupled to the electrodissolution of an array of Cr microbands present at the BPE anodes. The readout of this device is simple, where the species that dissolve the most Cr microbands are identified as the most promising electrocatalyst candidates for further evaluation. We demonstrate the utility of this technique by comparing several bi- and trimetallic systems involving Co, Fe, Ni, Mo, and W, which are compared directly with pure Pt. Of all the compositions tested, Ni_8−Mo_2 is demonstrated to be the most active for the HER in a neutral electrolyte solution.

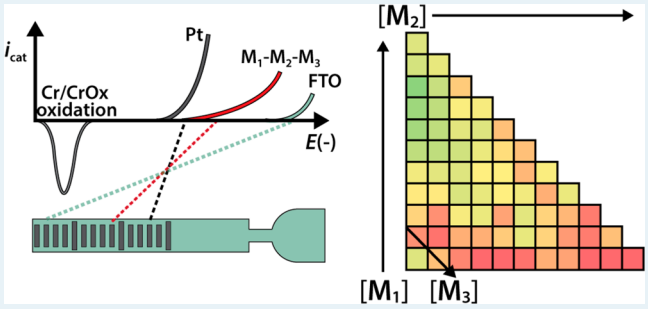

KEYWORDS: *electrochemistry, electrocatalysis, high-throughput screening*

INTRODUCTION

Here we report an electrocatalyst-screening platform for the hydrogen evolution reaction (HER) that is based on bipolar electrochemistry.[1−4] Specifically, combinations of Co, Fe, Mo, Ni, and W have been defined on the cathodic poles of arrays consisting of 36−72 individual bipolar electrodes (BPEs). These metallic composites are then screened by exposing the electrode array to an electric field present in an electrolyte solution. Because the HER, occurring at the BPE cathodes, is electrically coupled to anodic dissolution of Cr microbands present at the BPE anodes (Scheme 1a), superior electrocatalysts will result in electrodissolution of a large number of Cr microbands (Scheme 1b).[5] The number of bands dissolved is determined by optical microscopy.

High-throughput electrocatalyst screening techniques are typically carried out using one of three general schemes (or some combination thereof): (1) direct measurement of the amperometric or voltammetric behavior of the catalyst at individually addressable electrodes,[6−12] (2) interrogation of an array of materials using a scanning probe (e.g., a laser beam,[13] an optical fiber,[14−19] a movable reference and counter electrode,[10,20] or an ultramicroelectrode tip[17,21−27]) in serial format, or (3) detection of an optical signal change (e.g., changing local pH to turn on a fluorescent tracer,[28−30] changing reflectivity of a reporting thin film,[31,32] or monitoring gas bubbles[33]) arising from the products of an electrocatalyzed reaction. The direct measurement of current provides a great deal of information about the materials being evaluated but may become unwieldy with dense electrode arrays. Scanned probe techniques are very powerful, information-rich, and have been used in a variety of systems, but they are generally slow. Methods relying on an optical signal change offer much faster and simpler readout of the state of the array, but they may suffer from crosstalk between the materials being evaluated as a result of diffusion of the reporter dye. In addition, they do not provide as much information as the foregoing two methods.

Bipolar electrochemistry offers a convenient means for the parallel operation of large arrays of electrodes.[4,34,35] This is because each individual BPE is powered through an externally applied electric field. Accordingly, it is not necessary to connect each electrode to a power source or to directly measure current. However, because each BPE has both an anode and a cathode, an electrocatalytic reaction at one pole can be electrically linked to a reporting reaction at the other pole. For example, we previously showed that arrays of BPEs can be used to screen electrocatalysts for the oxygen reduction reaction (ORR) using

Received: February 7, 2014
Revised: March 17, 2014
Published: March 31, 2014

   dx.doi.org/10.1021/cs500168t | ACS Catal. 2014, 4, 1332−1339

Scheme 1. Schematic Representation of the BPE Screening Experiment and the Relationship between the Voltages Needed To Drive Both Cr Electrooxidation and the HER at Several Materials

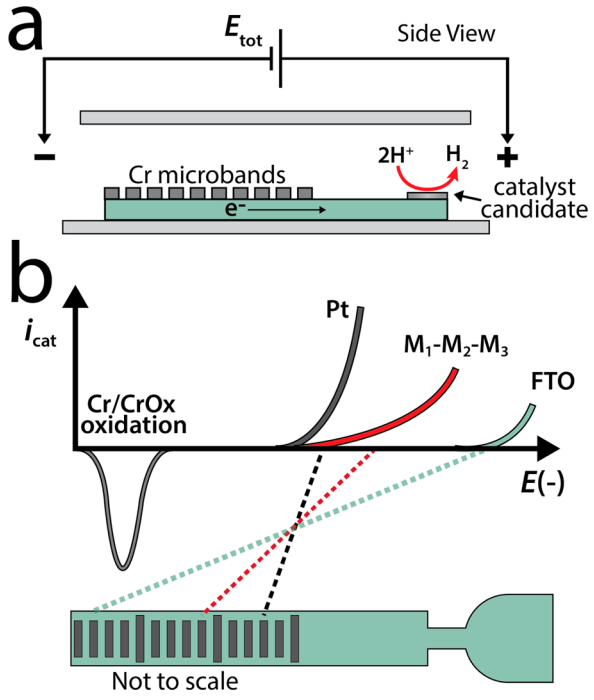

electrodissolution of thin metal films as the reporter reaction.[5,36] This provides a means for indirectly correlating the electrocatalytic current (or total charge) to the activity of the catalyst. Instead of measuring the absolute length change of a continuous film, we used arrays of microbands to determine the extent of the reaction. From a practical point of view, counting is easier than measuring length changes. Other groups have shown that electrogeneration of fluorescence or electrogenerated chemiluminescence (ECL) can be used to evaluate electrocatalysts using "closed" BPEs, in which the BPEs serve as the only electrical path between physically separated half cells.[35,37] Closed BPEs have also recently been used for electroanalysis within microdroplets, further improving miniaturization.[38] BPEs can also be used to prepare or screen material gradients.[39,40] The fundamentals of bipolar electrochemistry and the operating principles of sensing and screening applications have been discussed in recent reviews.[1,4]

Pd and Pt are considered benchmark materials for the HER because they have exchange current densities (j_0, A/cm^2) on the order of $\log(j_0) = -3$ A/cm^2.; however, they are scarce elements, making them impractical for large-scale applications.[41] In contrast, combinations of Co, Fe, Mo, Ni, and W might offer an economical alternative. For example, Co, Fe, Ni, Mo, and W have been tested individually and as composite materials for the HER in acidic and alkaline solutions, and the exchange current densities vary between $\log(j_0) = -6$ and -4 A/cm^2.[42−48] However, a direct comparison of these materials using consistent synthesis and measurement techniques has not been carried out, and there are conflicting reports as to which compositions are the most active for the HER. One such study showed that for Ni-containing materials, Ni−Mo was superior to Ni−Co and Ni−Fe.[42] Another study reported a lower overpotential for Co−Mo compared with Ni−Mo.[45] Others have shown that Ni−Mo outperforms Ni−Fe and Ni−W.[49] For the Ni−Mo system, some report a volcano-type relationship between activity and composition, with the maximum activity occurring near Ni/Mo = 1:1,[47] but others have found less systematic trends within narrow compositional variations.[46,48,49]

In the present study, we synthesized and directly compared the following bimetallic compositions: Fe−Mo, Co−Mo, Ni−Mo, Fe−Ni, Co−Ni, Ni−W, and Mo−W along with several trimetallic compositions: Ni−Mo−Fe, Ni−Mo−Co, and Ni−Mo−W. In all, we evaluated 231 different combinations of HER candidates. We found that most of these materials were unsuitable for use in acidic electrolytes compared with pure Pt. Under neutral conditions, however, we identified a compositional range of Ni−Mo materials (50−10% Mo) that produced promising results.

EXPERIMENTAL SECTION

Chemicals. Unless otherwise noted in the text, the following chemicals were used as received: $Fe(NO_3)_3{\cdot}9H_2O$ (Sigma Aldrich, 99.999%), $Co(NO_3)_2{\cdot}6H_2O$ (Alfa Aesar, 99.999%), $Ni(NO_3)_2{\cdot}6H_2O$ (Alfa Aesar, 99.9985%), $(NH_4)_6Mo_7O_{24}{\cdot}4H_2O$ (Sigma-Aldrich, 99.98%), $(NH_4)_{10}W_{12}O_{41}{\cdot}5H_2O$ (Sigma-Aldrich, 99.99%), $(NH_4)_2PtCl_4$ (Alfa Aesar, 99.9%), KH_2PO_4 (Fisher Scientific), and K_2HPO_4 (Fisher Scientific). All aqueous solutions were prepared using Milli-Q water (18.2 Ω·cm). For piezodispensing, the concentrations of the metal precursor solutions were 0.15 M (metal equivalent) in ethylene glycol (Fisher Scientific).

Device Fabrication and Design. The BPEs were microfabricated and consisted of fluorine-doped tin oxide (FTO, 12−14 Ω/sq, TEC15, 2 mm thick glass, Hartford Glass Co., Hartford City, IN) modified with Cr microbands, which were prepared using a slight modification of a previously described procedure.[5] Specifically, the etch step was longer (35 min) to account for the thickness of the FTO film. As shown in Scheme 1b, each BPE was 4.00 mm long and had a 325 μm-wide pad defining the cathodic pole. The functional anode of each BPE consisted of 100 individual Cr microbands (5 nm thick, 10 μm long, and 10 μm edge-to-edge spacing). The lateral spacing of BPEs in the array was 750 μm center-to-center. Arrays designed for screening bimetallic compositions consisted of 36 electrodes (3 rows of 12). Thirty-three of these electrodes were used to test bimetallic composites, varying in composition by 10 atomic percent, in triplicate. The remaining 3 electrodes were modified with Pt to serve as internal standards for each row. Arrays designed for screening trimetallic composites contained 72 electrodes: 66 electrodes for evaluating trimetallic composites in increments of 10 atomic percent, with the remaining 6 electrodes either modified with Pt (3−6 electrodes) or left as naked FTO (3−0 electrodes) to serve as controls.

Piezodispensing Materials. Precursor salt solutions were dispensed using a previously described piezodispensing setup.[15] The instrument has a printhead (PH46H-AT, Microfab) mounted onto an *x,y,z* robotic micropositioner (1560A, CH Instruments, Austin, TX). Each piezoelectric dispensing tip in the printhead is fed by a 2 mL reservoir connected to a pneumatic controller. The printhead contains four independent dispensing tips, so up to four components can be dispensed. Each electrode was modified with a total of 10 drops (~300 pL/drop) so that the total number of moles was maintained. By dispensing different relative numbers of drops of each precursor, the compositions can be changed by 10 atomic

dx.doi.org/10.1021/cs500168t | ACS Catal. 2014, 4, 1332−1339

percent. The geometrical fidelity of the array spots was evaluated by scanning electron microscopy (SEM) using a Zeiss Supra 40 VP microscope.

Bipolar Electrochemical Cell Configuration. Catalyst screening experiments were carried out using a bipolar electrochemical cell consisting of a pair of glassy carbon (GC) driving electrodes (separated by 28.6 mm); a silicone gasket (0.5 mm-thick, Grace Biolabs, Bend, OR), which was laser-cut (Epilog Zing 16, Epilog Laser, Golden, CO) to a width of either 12 mm or 19 mm depending on the size of the BPE array; and a microscope slide, which served as the bottom of the BPE cell. See Figure S1 in the Supporting Information for a schematic illustration of the cell configuration and device design. The BPE array, modified with electrocatalyst candidates, was then placed on top of this assembly with the electrodes facing down toward the microscope slide. The entire cell/electrode assembly was then placed into a home-built Teflon holder. Finally, the entire assembly was placed inside a transparent plastic box (16.4 × 12.1 × 4.8 cm, US Acrylic, LLC, Libertyville, IL) on a microscope stage.

The transparent box was purged with N_2 for at least 5 min before the cell was filled with electrolyte. Figure S2 in the Supporting Information shows the effectiveness of this purge box design for removing O_2, a possible source of background signal due to the ORR. A solution of 0.10 M PB (pH 6.9) was sparged with N_2 for at least 1 h before a small volume (~400 μL) was injected into the cell through a small opening in the purge box using a gastight syringe (500 μL, Hamilton) fitted with a small length of polyetheretherketone (PEEK) tubing.

Electrocatalyst Screening Experiments. The driving voltage (E_{tot})[4] was applied to the two GC driving electrodes using a programmable DC power supply (PWS4721, Tektronix, Portland, OR) controlled by a custom LabView program that enables custom voltage/current step programs as well as monitoring/recording the total current (i_{tot}) and applied voltage (E_{tot}) in real time.

In addition to the incorporation of dedicated Pt-modified BPEs as internal standards on each device, the strength of the electric field was measured during preliminary experiments using a pair of pyrolyzed photoresist film (PPF) microband electrodes[50] microfabricated on the bottom microscope slide and an electrometer (2700, Keithley Instruments, Cleveland, OH). As an additional quality check, the total current passing through the cell (i_{tot}) was collected from the power supply using the custom LabView program. Figure S3 in the Supporting Information shows the measured values of i_{tot} for the devices tested in 0.10 M PB (pH = 6.9) when E_{tot} = 17.5 V was applied for a 10 s duration. The average value of i_{tot} was 5.69 ± 0.14 mA, or a 2.5% variation, for eight independent experiments.

The experiments were monitored optically using a Nikon AZ100 microscope with a 0.5X PLAN APO objective. The camera was a Canon Rebel T3i digital single-lens reflex camera (DSLR) which was attached to the microscope using a Varimag II adapter (CNC Supply, Cape Coral, FL). Movies of the screening experiments were captured in the movie mode of the DSLR with a resolution of 1920 × 1080 pixels at a frame rate of 29.97 fps. This lower resolution but higher speed imaging was necessary given the short duration (10 s) of the screening experiment. This sacrifice in resolution means that the plots of bands removed vs time are measured by monitoring the dissolution of the slightly wider bands at 5-band intervals instead of counting individual bands.

Scale-up and Three-Electrode Experiments. Following the BPE screening experiments, macroscale films of certain compositions were synthesized and drop-cast onto electrodes for more detailed testing. Briefly, precursor solutions were premixed to a total concentration of 15 mM in ethylene glycol, and 225 μL aliquots of this solution were drop-cast onto 1.5 cm ×1.5 cm FTO substrates. Under 5% H_2/95% Ar flow, the drop-cast films were dried at 120 °C for 1 h and then annealed at 350 °C for 2 h. The electrochemical properties of the films were evaluated in a three-electrode cell outfitted with a Pt wire counter electrode and a Ag/AgCl (saturated KCl, E = 0.197 V vs NHE) reference electrode. The cell was filled with an electrolyte solution consisting of N_2-sparged 0.20 M PB (pH 6.9), and it was controlled by a potentiostat (601D, CH Instruments, Austin, TX). All potentials are converted from V vs Ag/AgCl to the potential of a reversible hydrogen electrode (RHE, E = −0.408 V vs NHE at pH = 6.9) to simplify comparison with the scientific literature.

RESULTS AND DISCUSSION

Principles of the Screening Experiments. BPEs are well-suited for array-based sensing and screening experiments because an entire array can be powered by a single power source and because a direct electrical connection to each BPE is not required. The basic principles and fundamentals of bipolar electrochemistry have been discussed in detail in recent reviews,[1,4] but the specific operating principles of a BPE screening experiment are described next.

As shown in Scheme 1a, a potential bias (E_{tot}) is applied between a pair of driving electrodes to produce an electric field in the solution covering the BPE array. The fraction of E_{tot} dropped over each electrode is referred to as ΔE_{elec}, and the latter is estimated by multiplying the length of the BPE by the strength of the electric field. ΔE_{elec} is the driving force for the faradaic reactions occurring at the two poles of each BPE. When E_{tot} is first applied, all of the BPEs in the array experience the same magnitude of ΔE_{elec}. However, as the Cr microbands begin to dissolve, the effective length of each BPE in the array decreases, thereby decreasing ΔE_{elec}. Because both the oxidation of the Cr microbands and the HER must be driven simultaneously, when ΔE_{elec} becomes too small, the two reactions effectively stop. Better electrocatalysts need lower overpotentials to drive the reaction and, thus, oxidize more Cr microbands, thereby providing a permanent record of the outcome of the screen. Cr was chosen as an anodic reporter because it is easy to microfabricate, is stable during catalyst candidate preparation, and is electroactive under a variety of solution conditions.

Short duration BPE screening experiments. In our previous report of screening ORR electrocatalysts, the experiment was allowed to progress for up to 5 min so that the rate of Cr dissolution effectively stopped. This made it possible to determine the relative onset potentials for the ORR by simply counting the number of Cr microbands that dissolved. However, for the screening experiments reported here, we have adopted a slightly different approach.

Instead of allowing the reactions to progress until the rates become insignificant, we apply E_{tot} for a much shorter time (5 or 10 s, depending on the electrolyte). The motivation behind this change in experimental protocol is to remove, to the maximum extent possible, contributions of background processes, such as the ORR, that could affect the apparent end point of the experiment. In many systems, the HER occurs

dx.doi.org/10.1021/cs500168t | ACS Catal. 2014, 4, 1332−1339

at a much faster rate than the ORR, especially in the N_2-purged electrolyte solutions used in the experiments reported here.

The important distinction between the short-duration screening experiments used here and the longer durations used previously is that instead of determining a relative onset potential for the electrocatalytic reaction of interest, the screening experiment is ended while both the anode and cathode reactions are active. This is analogous to determining the overpotential at a particular current density rather than determining the onset potential for the reaction. Therefore, it is very important to select an appropriate duration for the application of E_{tot}.

In a preliminary experiment, using Ni−Mo as a bimetallic catalyst in 0.10 M PB (pH 6.9), E_{tot} was applied for 30 s, and the rate of Cr microband dissolution was measured as a function of time. Figure 1a is an optical micrograph of one row of a BPE array consisting of 36 individual electrodes (3 rows of 12 electrodes each) configured such that a bimetallic system of 10% compositional variation can be evaluated in triplicate (33 total electrodes) with the 3 remaining electrodes modified with piezodispensed Pt serving as a control. Parts b and c of Figure 1 show the progress of the screening experiment during the application of E_{tot} = 17.5 V for 10 and 30 s, respectively. These data demonstrate that the majority of dissolution occurs within the first 10 s, with just 1−5 bands dissolving during the remaining 20 s. Therefore, the duration of all experiments carried out in PB electrolyte was limited to 10 s.

Figure 2a is a plot of the number of bands removed as a function of time for the electrodes shown in Figure 1. These data indicate that the rate of dissolution of the Cr microbands from the anodic pole of each electrode is related to the material present at the cathode. The electrode modified with Pt (black) dissolves the most bands during the application of E_{tot}. The Ni−Mo composites that dissolved the most bands within the first 10 s consisted of 40−50% Ni. Figure 2b is a plot of the electric field strength, measured between two PPF microbands fabricated on the bottom glass piece of the bipolar electrochemical cell, and i_{tot}, the total current flowing in the cell as a function of time. A comparison of these data indicates that there is a time-dependent decay in both i_{tot} and the strength of the electric field across the cell. The important point is that within 5 s, both the current and the field are stabilized, and hence, times >5 s are desirable for making reproducible measurements.

Demonstrating Reproducibility with Piezodispensed Pt. To determine the reproducibility of this screening approach, a control experiment was carried out by evaluating the HER on 36 nominally identical BPEs. Figure 3a is an optical micrograph of one row of the array, comprising 12 BPEs, prior to application of E_{tot}. Parts b and c of Figure 3 show the device during the applied potential pulse at t = 5 and 10 s. The red bars indicate the position of lowest intact Cr microband. At the conclusion of the 10 s duration of the experiment, an average of 45.1 ± 1.8 Cr microbands dissolved. In an independent, replicate experiment, the average number of Cr microbands dissolved was 43.2 ± 1.8. Altogether, a total of 99 Pt spots were tested in the PB electrolyte, and 46 ± 4 microbands were found to dissolve. These results demonstrate that the level of reproducibility is around 10% using this short potential pulse method. This value is comparable to the variability reported previously for the long potential pulse method applied to ORR electrocatalyst candidates. The error probably results from several contributions: (1) the precise location of the materials at the BPE cathode, (2) the reproducibility of the cell configuration, and (3) the true electrochemical nature of the electrocatalyst candidates.[4]

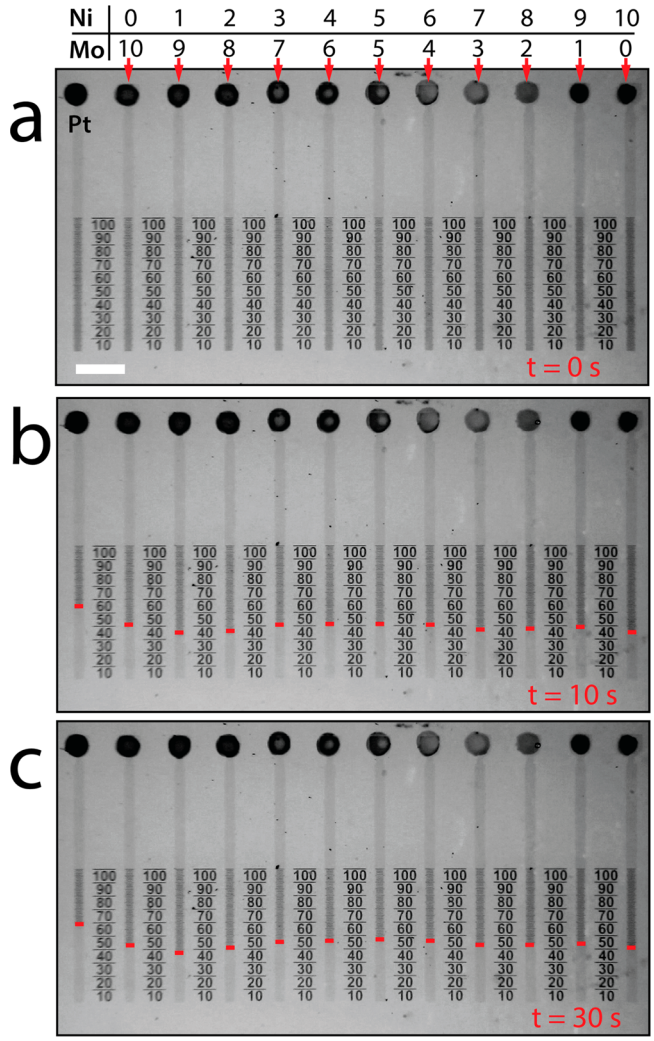

Figure 1. A BPE electrochemical cell for screening Ni−Mo bimetallic catalyst candidates for the HER. (a) Optical micrograph of the device prior to the application of E_{tot}. Each electrode in the array is 4.00 mm long and has a cathodic pad that is 325 μm wide. The anodic pole of each electrode was modified with an array of 100 individual Cr microbands. The cathodic pole of the left-most electrode was modified with 10 drops of Pt. The remaining electrodes were modified with the indicated number of drops of precursor solution for Mo and Ni such that the total number of moles of metal (Ni + Mo) deposited on each electrode was the same, but the atomic percentages varied by 10%. The silicone gasket used to define the walls of the fluidic space was 12 mm wide. E_{tot} = 17.5 V was applied for 30 s. The remaining frames show the progress of the screening experiment at (b) 10 s and (c) 30 s. The movie from which these frames were extracted is included in the Supporting Information (movie 1).

Figure 4a provides additional information regarding reproducibility. It is a plot of the number of Cr microbands removed as a function of time throughout the 10 s duration of the experiment. The data for each electrode were fitted using a single exponential function to compare the rates of dissolution. At short times (50 to 500 ms), the rates show decreasing relative standard deviations (RSDs) from 7 to 12% across the 12 electrodes. At longer times (t > 500 ms), the RSDs of the

dx.doi.org/10.1021/cs500168t | ACS Catal. 2014, 4, 1332−1339

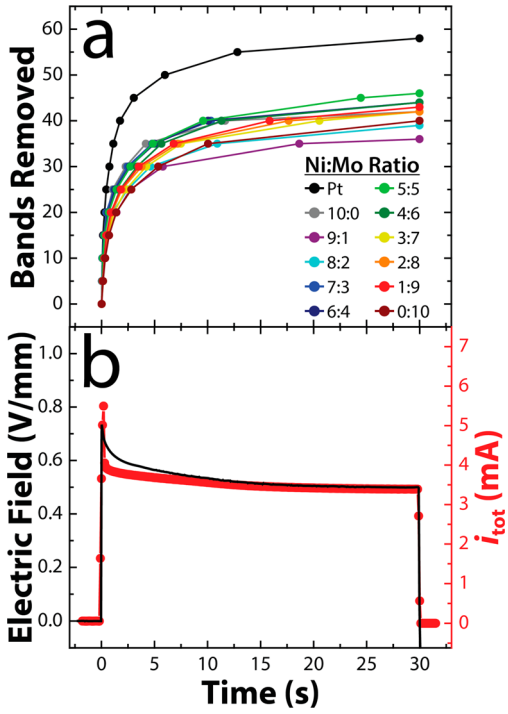

Figure 2. (a) Plot of the number of Cr bands removed vs time for the same device shown in Figure 1. (b) Electric field strength (black, left axis) and total current (i_{tot}, red, right axis) flowing through the electrochemical cell as a function of time during the application of E_{tot} = 17.5 V. The field strength was measured using a pair of PPF microbands (150 μm wide, separated by 20 mm) fabricated onto the bottom microscope slide of the bipolar electrochemical cell. Notice the time-dependent decay of i_{tot} and the electric field strength during the application of E_{tot}.

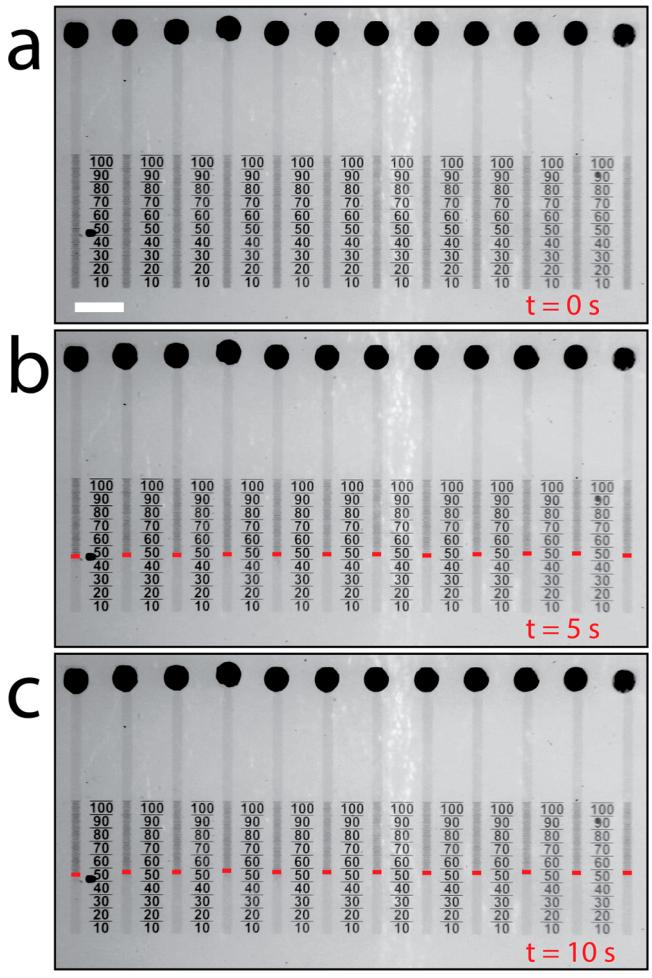

Figure 3. A BPE electrochemical cell for screening Pt candidates for the HER. (a) Optical micrograph of the device prior to the application of E_{tot}. The configuration of the BPE array is the same as in Figure 1, except here, every BPE on this device was modified with Pt. The silicone gasket used to define the walls of the fluidic space was 19 mm wide. E_{tot} = 17.5 V was applied for 10 s. The remaining frames show the progress of the screening experiment at (b) 5 s and (c) the 10 s. The movie from which these frames were extracted is included in the Supporting Information (movie 2).

rates of dissolution are <5%. Figure 4b shows the electric field strength and i_{tot} during the E_{tot} pulse.

We carried out screening experiments similar to those just described, but in 50 mM H_2SO_4 for an array of BPEs modified with Pt. Under these conditions, the average for all piezodispensed Pt spots evaluated, using a 5 s pulse of E_{tot} = 15.0 V in the 50 mM H_2SO_4 electrolyte (42 total), was 48 ± 5 Cr microbands dissolved. An example of a screening experiment for piezodispensed Pt is shown in Figure S4 in the Supporting Information.

Screening Bi- and Trimetallic Nonnoble Metal Electrocatalyst Candidates. After demonstrating that the selected experimental design and operating parameters result in reproducible data for Pt alone, we returned to evaluating bi- and trimetallic compositions for the HER using 0.10 M PB (pH 6.9) electrolyte and Ni and Mo as the common elemental components. Each bimetallic composition was evaluated in triplicate, and Pt served as an internal standard for each row to provide reliable intra- and interdevice comparisons. The BPE arrays used for testing trimetallic materials consisted of 3 rows of 24 individual electrodes (72 total electrodes). Sixty-six of the electrodes were modified with a mono-, bi-, or trimetallic mixture of Ni−Mo−M, where M = Co, Fe, or W, and the remaining electrodes were either modified with Pt or left as naked FTO to serve as controls.

Figure 5 shows matrix plots for 3 different trimetallic combinations: Ni−Mo−Co, Ni−Mo−Fe, and Ni−Mo−W. These plots show the number of Cr microbands dissolved for each species and are color-coded according to the scale shown on the right: dark green tones represent the best catalysts. The arrays vary in atomic composition by 10% for Ni on the vertical axis, by 10% for Mo on the diagonal (indicated by thin black dashed lines), and by 10% for the third metal on the horizontal axis. A total of 10 drops was used to prepare each trimetallic composite. For example, Figure 5a shows the results for the Ni−Mo−Co trimetallic. To identify the performance of Ni_6−Mo_2−Co_2, start with the row designating 6 drops of Ni, then find the column indicating 2 drops of Co, and then follow the diagonal black dashed line to the box indicating 2 drops of Mo. The results for this material are found in the box highlighted by a red border (30 bands removed). Several reports indicate that trimetallic composites of Ni−Mo−Co may outperform Ni−Mo or the monometallics.[51,52] In addition, Co−Mo has been reported to require a lower overpotential for the HER than Ni−Mo.[45] In our case, however, the bimetallic Ni−Mo catalysts were the most active species with generally decreasing performance as the percentage of Ni was lowered. It is also important to point out that the differences in the number of Cr bands dissolved is low within certain compositional windows,

dx.doi.org/10.1021/cs500168t | ACS Catal. 2014, 4, 1332−1339

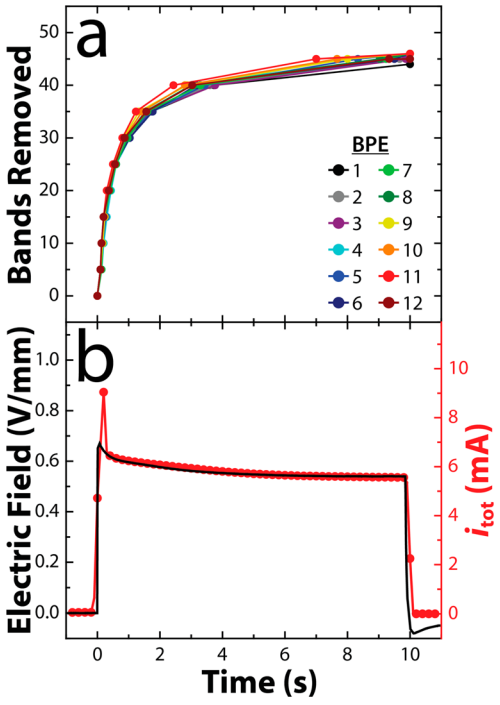

Figure 4. (a) Plot of the number of Cr bands removed vs time for the same device shown in Figure 3. (b) Electric field strength (black, left axis) and total current (i_{tot}, red, right axis) flowing through the electrochemical cell as a function of time during the application of E_{tot} = 17.5 V. The field strength was measured using a pair of PPF microbands (150 μm wide, separated by 20 mm) fabricated onto the bottom microscope slide of the bipolar electrochemical cell. Notice the time-dependent decay of i_{tot} and the electric field strength during the application of E_{tot}.

but these results are still useful for identifying trends in the performance of the materials.

Figure 5b shows results for the Ni−Mo−Fe trimetallic system. In basic electrolyte solutions, Ni−Mo−Fe has been reported to have higher activities than the other trimetallic compositions tested here.[52] As is evident from this matrix, the bimetallic Ni−Mo system produced the most active species, with low (less than 30%) amounts of Fe producing similar numbers of Cr bands removed, suggesting that additional, more detailed studies of these materials might be warranted.

Figure 5c shows the screening results for the Ni−Mo−W trimetallic system. W was chosen as the third component on the basis of its slightly higher exchange current density than Mo: $\log(j_0) \approx -6$ A/cm^2 vs -7 A/cm^2.[43] Interestingly, high concentrations of W appear to produce poorly performing materials, and composites with small amounts of W (less than 30%) showed performance similar to the bimetallic Ni−Mo system.

In this study, the bimetallic Ni−Mo catalysts (left-most columns in Figure 5) consistently performed better than the three trimetallic combinations. Figure 6 shows the results of the Ni−Mo system in the PB and H_2SO_4 electrolytes. The dark gray bars in Figure 6 summarize the relative activity of the Ni−Mo materials (tested in 0.10 M PB, pH 6.9) for at least 8 independently prepared electrodes for each composition. The most active species was Ni_8−Mo_2, but all of the compositions consisting of between 50 and 90% Ni exhibited better average activity than the pure component metals. This result is consistent with a recent study of Ni−Mo nanopowders.[53]

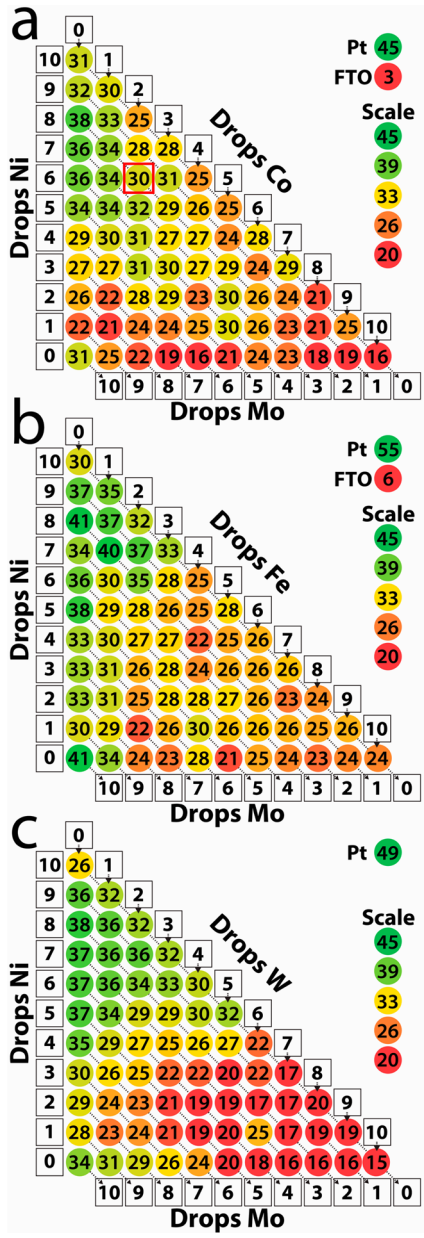

Figure 5. Matrix plot showing the number of Cr bands dissolved as a function of composition for bimetallic and trimetallic catalysts. The vertical axis represents the number of drops of the Ni precursor dispensed, the diagonal axis (bottom, indicated by black dashed arrows) corresponds to Mo, and the horizontal axis to the third catalyst component for (a) Ni−Mo−Co, (b) Ni−Mo−Fe, and (c) Ni−Mo−W. The numbers in the chart indicate the average number of bands dissolved for two independent experiments. To more intuitively spot trends, the data are color coded according to the legend to the right of each figure. The average performance of the Pt and naked FTO support is shown on the right side of the plot. See main text for an example of how to read the matrixes.

The light gray bars in Figure 6 correspond to the same Ni−Mo combinations described in the previous paragraph, except now evaluated for activity using 50 mM H_2SO_4 electrolyte. There were differences in performance across the compositional range, but the materials performed considerably worse than Pt, and all compositions performed more poorly than in PB buffer. Furthermore, even in the short amount of time necessary to run the screening experiment (~3−5 min), the

dx.doi.org/10.1021/cs500168t | ACS Catal. 2014, 4, 1332−1339

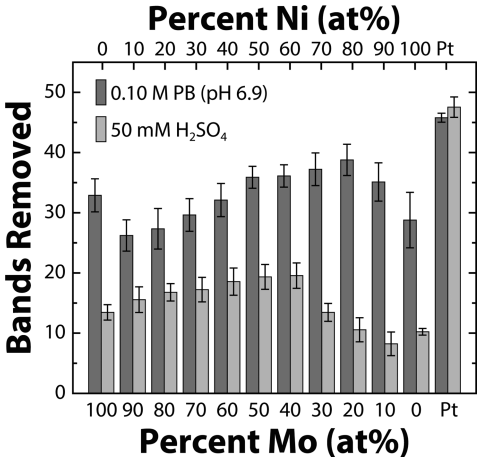

Figure 6. Bar graph showing the number of Cr microbands dissolved for the bimetallic Ni−Mo system in 0.10 M PB (pH 6.9) (dark gray) and 50 mM H_2SO_4 (light gray). The bars on the far right indicate the mean performance of Pt over all devices in each electrolyte. The error bars indicate the 95% confidence interval for these data.

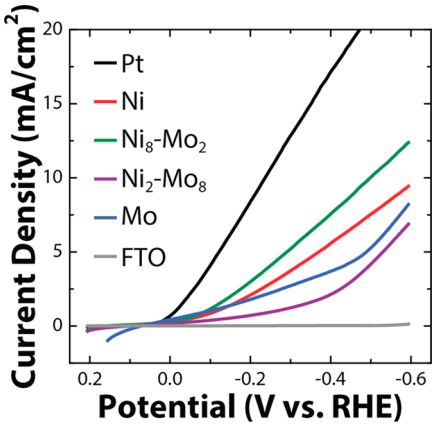

Figure 7. LSV scans for macroscale metal films of materials indicated in the legend. The electrolyte was 0.20 M PB (pH 6.9), which was continuously sparged with N_2 gas. The initial scan direction was negative. The scan rate was 25 mV/s, and no *iR* compensation was used.

materials partially dissolved from the cathodic pole in the acidic electrolyte. This poor stability has been predicted for Ni- and Mo-based materials via density functional theory (DFT) calculations.[54] The results for bimetallic Fe−Mo and Co−Mo combinations in the acidic electrolyte are provided in the Supporting Information (Figure S5). Both systems suffered from inconsistent results and showed no enhancement over the monometallic materials.

One disadvantage of synthesizing metals by piezoelectric dispensing of metal salt solutions followed by reduction at elevated temperatures is that the surface structure and morphology are not controlled. Therefore, differences in activity for various piezoelectric dispensed compositions may be partially due to differences in the accessible surface area of the catalyst.[55] To address this concern, we viewed the Ni−Mo array spots, along with the Pt spots and naked FTO, by SEM (Figures S6 and S7 in the Supporting Information). The SEM micrographs reveal a somewhat porous nanostructure for pure Ni, Mo, and Pt; however, the bimetallic Ni−Mo compositions (10−90% Mo) appear to be mostly dense without a remarkable amount of surface structure. Therefore, compositional effects likely play a larger role in the catalytic activity of the Ni−Mo system than surface area. However, the nature of screening experiments is such that more detailed structural and compositional studies are carried out on only the most promising candidates rather than on the entire array of materials.

Three-Electrode Evaluation of Ni−Mo. Because the Ni−Mo bimetallics containing 50−80% Ni reproducibly yielded the most active catalysts, we prepared macroscale films of several Ni−Mo compositions (0, 20, 80, and 100% Mo) by drop-casting the appropriate metal salts and then heating in H_2 to verify the results obtained from the screening experiments. A three-electrode electrochemical cell and the technique of linear scan voltammetry (LSV) were used for these measurements. The results are shown in Figure 7.

The LSV trace for Pt shows a cathodic current onset near the thermodynamic potential for the HER (0 V vs RHE). The Ni_8−Mo_2 bimetallic exhibited a similar cathodic current onset potential, but a slower increase in current density compared with Pt. At a current density of 10 mA/cm^2, Pt had the lowest HER overpotential (237 mV), followed by Ni_8−Mo_2 (498 mV). Ni_2−Mo_8 and Mo yielded significantly higher HER overpotentials and did not reach 10 mA/cm^2 at potentials more positive than −0.6 V vs RHE. The important point is that the LSV results, obtained using a traditional electrochemical setup and macroscale electrodes, are consistent with the results of BPE screening experiments (Figure 6), verifying that the BPE screening platform can be used to select promising electrocatalyst candidates for the HER.

SUMMARY AND CONCLUSIONS

We have demonstrated that bipolar electrochemistry can be used to evaluate electrocatalyst candidates for the HER. Specifically, a series of bi- and trimetallic candidates were prepared using a piezodispensing technique followed by chemical reduction, and the resulting materials were tested in both neutral and acidic electrolytes. Better stability was observed in neutral electrolytes, and the most active material identified was a Ni−Mo bimetallic consisting of 20% Mo. Although this study focuses on the performance of electrocatalyst candidates for the HER in acidic and neutral electrolyte solutions, we hypothesize that such screening experiments can also be carried out in basic electrolytes. The fact that the catalytic activity of these materials is consistent with that found using LSV, as well as results reported by other groups who used different screening methods, is a reassuring sign that BPE screening provides accurate results.

The key point is that a large number of catalyst compositions can be screened in just a few minutes using simple instrumentation and that the BPE screening method leaves a permanent record of the results. Moreover, by filming videos of the dissolution of the Cr bands, it is possible to obtain kinetic data about the catalyst. Indeed, we are presently trying to understand how such videos can accurately be converted into quantitative kinetic information. This turns out to be a complicated problem, but if it can be resolved, this approach to screening will become even more useful.

ASSOCIATED CONTENT

Supporting Information

Movie of the HER on BPEs modified with Ni−Mo and Pt in PB, schematic representations of the BPE cell and electrodes,

dx.doi.org/10.1021/cs500168t | ACS Catal. 2014, 4, 1332−1339

measurement of O_2 levels in the purge box; measured values of i_{tot} as a function of time for catalysts evaluated using PB, frames showing the HER at BPEs modified with Pt in 50 mM H_2SO_4, activity of bimetallic Fe−Mo and Co−Mo in 50 mM H_2SO_4, SEM micrographs of different Ni−Mo compositions. This material is available free of charge via the Internet at http://pubs.acs.org.

AUTHOR INFORMATION

Corresponding Authors

*E-mail: mullins@che.utexas.edu.
*E-mail: crooks@cm.utexas.edu.

Author Contributions

§S.E.F. and S.P.B. contributed equally to this work.

Notes

The authors declare no competing financial interest.

ACKNOWLEDGMENTS

The authors gratefully acknowledge financial support from the Chemical Sciences, Geosciences, and Biosciences Division, Office of Basic Energy Sciences, Office of Science, U.S. Department of Energy (S.E.F. and R.M.C., Contract No. DE-FG02-06ER15758; S.P.B. and C.B.M., Contract No. DE-FG02-04ER15587). The Robert A. Welch Foundation provides sustained support for our research (Grant F-0032 for R.M.C. and F-1436 for C.B.M.). We also thank Tim Hooper at UT-Austin for his help with the custom LabView program.

REFERENCES

(1) Mavré, F.; Anand, R. K.; Laws, D. R.; Chow, K.-F.; Chang, B.-Y.; Crooks, J. A.; Crooks, R. M. *Anal. Chem.* **2010**, *82*, 8766−8774.
(2) Loget, G.; Kuhn, A. *Anal. Bioanal. Chem.* **2011**, *400*, 1691−1704.
(3) Loget, G.; Zigah, D.; Bouffier, L.; Sojic, N.; Kuhn, A. *Acc. Chem. Res.* **2013**, *46*, 2513−2523.
(4) Fosdick, S. E.; Knust, K. N.; Scida, K.; Crooks, R. M. *Angew. Chem., Int. Ed.* **2013**, *52*, 10438−10456.
(5) Fosdick, S. E.; Berglund, S. P.; Mullins, C. B.; Crooks, R. M. *Anal. Chem.* **2013**, *85*, 2493−2499.
(6) Sullivan, M. G.; Utomo, H.; Fagan, P. J.; Ward, M. D. *Anal. Chem.* **1999**, *71*, 4369−4375.
(7) Guerin, S.; Hayden, B. E.; Lee, C. E.; Mormiche, C.; Owen, J. R.; Russell, A. E.; Theobald, B.; Thompsett, D. *J. Comb. Chem.* **2004**, *6*, 149−158.
(8) Strasser, P.; Fan, Q.; Devenney, M.; Weinberg, W. H.; Liu, P.; Nørskov, J. K. *J. Phys. Chem. B* **2003**, *107*, 11013−11021.
(9) He, T.; Kreidler, E.; Xiong, L.; Ding, E. *J. Power Sources* **2007**, *165*, 87−91.
(10) Lee, K. R.; Jeon, M. K.; Woo, S. I. *Appl. Catal., B* **2009**, *91*, 428−433.
(11) Dang, T.; Ramsaran, R.; Roy, S.; Froehlich, J.; Wang, J.; Kubiak, C. P. *Electroanalysis* **2011**, *23*, 2335−2342.
(12) Zhang, Y.; McGinn, P. J. *J. Power Sources* **2012**, *206*, 29−36.
(13) Woodhouse, M.; Parkinson, B. A. *Chem. Mater.* **2008**, *20*, 2495−2502.
(14) Liu, G.; Bard, A. J. *J. Phys. Chem. C* **2010**, *114*, 17509−17513.
(15) Berglund, S. P.; Lee, H. C.; Nunez, P. D.; Bard, A. J.; Mullins, C. B. *Phys. Chem. Chem. Phys.* **2013**, *15*, 4554−65.
(16) Liu, G.; Liu, C.; Bard, A. J. *J. Phys. Chem. C* **2010**, *114*, 20997−21002.
(17) Ye, H.; Lee, J.; Jang, J. S.; Bard, A. J. *J. Phys. Chem. C* **2010**, *114*, 13322−13328.
(18) Ye, H.; Park, H. S.; Bard, A. J. *J. Phys. Chem. C* **2011**, *115*, 12464−12470.
(19) Zhang, F.; Roznyatovskiy, V.; Fan, F.-R. F.; Lynch, V.; Sessler, J. L.; Bard, A. J. *J. Phys. Chem. C* **2011**, *115*, 2592−2599.
(20) Lee, K. R.; Jung, Y.; Woo, S. I. *ACS Comb. Sci.* **2011**, *14*, 10−16.
(21) Weng, Y.-C.; Hsieh, C.-T. *Electrochim. Acta* **2010**, *56*, 1932−1940.
(22) Fernández, J. L.; Raghuveer, V.; Manthiram, A.; Bard, A. J. *J. Am. Chem. Soc.* **2005**, *127*, 13100−13101.
(23) Fernández, J. L.; Walsh, D. A.; Bard, A. J. *J. Am. Chem. Soc.* **2005**, *127*, 357−365.
(24) Fernández, J. L.; White, J. M.; Sun, Y. M.; Tang, W. J.; Henkelman, G.; Bard, A. J. *Langmuir* **2006**, *22*, 10426−10431.
(25) Li, W.; Fan, F.-R. F.; Bard, A. J. *J. Solid State Electrochem.* **2012**, *16*, 2563−2568.
(26) Walsh, D. A.; Fernández, J. L.; Bard, A. J. *J. Electrochem. Soc.* **2006**, *153*, E99−E103.
(27) Johnson, L.; Walsh, D. A. *J. Electroanal. Chem.* **2012**, *682*, 45−52.
(28) Reddington, E.; Sapienza, A.; Gurau, B.; Viswanathan, R.; Sarangapani, S.; Smotkin, E. S.; Mallouk, T. E. *Science* **1998**, *280*, 1735−1737.
(29) Chai, G. S.; Yu, J.-S. *J. Mater. Chem.* **2009**, *19*, 6842−6848.
(30) Welsch, F. G.; Stowe, K.; Maier, W. F. *ACS Comb. Sci.* **2011**, *13*, 518−529.
(31) Jaramillo, T. F.; Ivanovskaya, A.; McFarland, E. W. *J. Comb. Chem.* **2001**, *4*, 17−22.
(32) Brace, K. M.; Hayden, B. E.; Russell, A. E.; Owen, J. R. *Adv. Mater.* **2006**, *18*, 3253−3257.
(33) Xiang, C.; Suram, S. K.; Haber, J. A.; Guevarra, D. W.; Soedarmadji, E.; Jin, J.; Gregoire, J. M. *ACS Comb. Sci.* **2014**, *16*, 47−52.
(34) Chow, K.-F.; Mavré, F.; Crooks, J. A.; Chang, B.-Y.; Crooks, R. M. *J. Am. Chem. Soc.* **2009**, *131*, 8364−8365.
(35) Guerrette, J. P.; Percival, S. J.; Zhang, B. *J. Am. Chem. Soc.* **2013**, *135*, 855−61.
(36) Fosdick, S. E.; Crooks, R. M. *J. Am. Chem. Soc.* **2012**, *134*, 863−866.
(37) Lin, X.; Zheng, L.; Gao, G.; Chi, Y.; Chen, G. *Anal. Chem.* **2012**, *84*, 7700−7707.
(38) Wu, S. Z.; Zhou, Z. Y.; Xu, L. R.; Su, B.; Fang, Q. *Biosens. Bioelectron.* **2014**, *53*, 148−153.
(39) Ramaswamy, R.; Shannon, C. *Langmuir* **2010**, *27*, 878−881.
(40) Munktell, S.; Tyden, M.; Hogstrom, J.; Nyholm, L.; Bjorefors, F. *Electrochem. Commun.* **2013**, *34*, 274−277.
(41) Yang, C.-J. *Energy Policy* **2009**, *37*, 1805−1808.
(42) Raj, I. A. *J. Mater. Sci.* **1993**, *28*, 4375−4382.
(43) Trasatti, S. *J. Electroanal. Chem. Interfacial Electrochem.* **1972**, *39*, 163−184.
(44) Miles, M. H. *J. Electroanal. Chem. Interfacial Electrochem.* **1975**, *60*, 89−96.
(45) Fan, C.; Piron, D. L.; Paradis, P. *Electrochim. Acta* **1994**, *39*, 2715−2722.
(46) Highfield, J. G.; Claude, E.; Oguro, K. *Electrochim. Acta* **1999**, *44*, 2805−2814.
(47) Jakšić, J. M.; Vojnović, M. V.; Krstajić, N. V. *Electrochim. Acta* **2000**, *45*, 4151−4158.
(48) Gennero de Chialvo, M. R.; Chialvo, A. C. *J. Electroanal. Chem.* **1998**, *448*, 87−93.
(49) Navarro-Flores, E.; Chong, Z.; Omanovic, S. *J. Mol. Catal. A: Chem.* **2005**, *226*, 179−197.
(50) Dumitrescu, I.; Yancey, D. F.; Crooks, R. M. *Lab Chip* **2012**, *12*, 986−993.
(51) Arce-Estrada, E.; Lopez-Hirata, V.; Martinez-Lopez, L.; Dorantes-Rosales, H.; Saucedo-Muñoz, M.; Hernández-Santiago, F. *J. Mater. Sci.* **2003**, *38*, 275−278.
(52) Raj, I. A.; Vasu, K. I. *J. Appl. Electrochem.* **1992**, *22*, 471−477.
(53) McKone, J. R.; Sadtler, B. F.; Werlang, C. A.; Lewis, N. S.; Gray, H. B. *ACS Catal.* **2013**, *3*, 166−169.
(54) Greeley, J.; Nørskov, J. K. *Surf. Sci.* **2007**, *601*, 1590−1598.
(55) Trasatti, S.; Petrii, O. A. *J. Electroanal. Chem.* **1992**, *327*, 353−376.